Glomsda *et al. Earth, Planets and Space* (2022) 74:87
https://doi.org/10.1186/s40623-022-01634-1

Earth, Planets and Space

FULL PAPER

Comparison of non-tidal loading data for application in a secular terrestrial reference frame

Matthias Glomsda*, Mathis Bloßfeld, Manuela Seitz, Detlef Angermann and Florian Seitz

Abstract

The Deutsches Geodätisches Forschungsinstitut der Technischen Universität München (DGFI-TUM) is one of the three Combination Centres of the International Earth Rotation and Reference Systems Service for the International Terrestrial Reference System (ITRS). In its upcoming realization of the ITRS, the DTRF2020, DGFI-TUM will again correct for non-tidal loading (NTL) effects at the normal equation level. Next to the dedicated NTL data set for the ITRS 2020 realization provided by the Global Geophysical Fluid Center (GGFC), we also considered the data provided by the Earth System Modelling group of the Deutsches GeoForschungsZentrum (ESMGFZ). Besides also comprising all NTL components (atmospheric, oceanic, hydrological) and being mass conserving, the ESMGFZ data has the advantage of daily availability and is already in use at DGFI-TUM. The decision for one or the other data set depends on their suitability for a secular terrestrial reference frame like the DTRF2020, which will be assessed in this work. Although we also compare the site displacements induced by NTL to the residuals of station positions of the Global Navigation Satellite Systems, we will not evaluate the quality of the underlying geophysical models per se. The two data sets differ w.r.t. the underlying hydrological models and the treatment of non-tidal oceanic loading, but the most relevant difference is given in terms of trends in the displacement time-series. After a close investigation of the latter, we finally decided to apply the GGFC contribution to the ITRS 2020 realization in the DTRF2020.

Keywords: Terrestrial reference frame, DTRF, Non-tidal loading, Site displacements, GGFC, ESMGFZ

*Correspondence: matthias.glomsda@tum.de

Deutsches Geodätisches Forschungsinstitut der Technischen Universität München (DGFI-TUM), Arcisstraße 21, 80333 München, Germany

Graphical Abstract

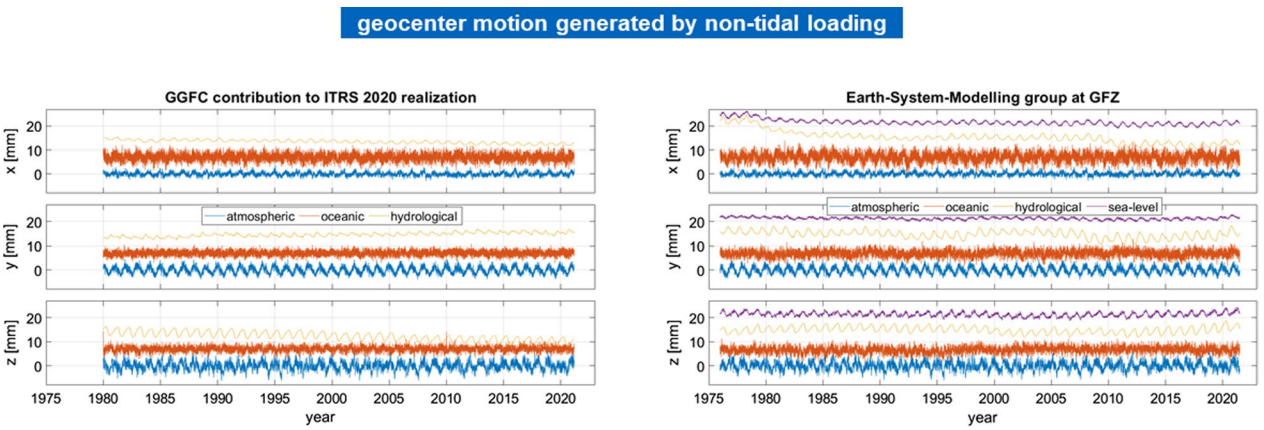

Introduction

Every 5–6 years, new realizations of the International Terrestrial Reference System (ITRS) are computed by the ITRS Combination Centres (CC) of the International Earth Rotation and Reference Systems Service (IERS). These realizations are called terrestrial reference frames (TRF), and the CC are the Institut national de l'information géographique et forestière (IGN) in France, NASA's Jet Propulsion Laboratory (JPL) in the USA, and the Deutsches Geodätisches Forschungsinstitut der Technischen Universität München (DGFI-TUM) in Germany. The ITRS is a conventional 3-dimensional Cartesian reference system co-rotating with the Earth, in which the x- and y-coordinate axes lie in the conventional equatorial plane, with the x-axis pointing towards the Greenwich meridian, and the z-axis is oriented to the IERS reference pole. The origin is identical to the centre of mass of the total Earth system including the oceans and the atmosphere. The scale of the ITRS is defined to be the SI meter (e.g., Petit and Luzum 2010).

The ITRS is realized by the positions of reference points w.r.t. this system. These reference points belong to the observing stations of the four geodetic space techniques: Very Long Baseline Interferometry (VLBI), Satellite Laser Ranging (SLR), the Global Navigation Satellite Systems (GNSS), and Doppler Orbitography and Radiopositioning Integrated by Satellite (DORIS). By applying conventional correction models (Petit and Luzum 2010) for geophysical effects like Earth tides, ocean tides, and tidal loading, the corresponding station motions can be reduced (or regularized) to a long-term linear motion with non-linear residuals. The realizations by IGN (e.g., ITRF2014; Altamimi et al. 2016) and DGFI-TUM (e.g., DTRF2014; Seitz et al. 2021) provide respective 3-dimensional position (at a specific reference epoch) and velocity vectors for each participating station, and hence represent secular reference frames. The realization by JPL (e.g., JTRF2014; Abbondanza et al. 2017), however, does not apply this parameterization but provides station position time-series instead.

In this study, we focus on the secular reference frames. The analysis of station position time-series reveals remaining (unmodelled) non-linear effects, that are still a major limiting factor for the accuracy of long-term reference frames. Such non-linear motions are induced by technique-specific effects like, e.g., the gravitational deformation of VLBI antennas (Nothnagel et al. 2019), or by geophysical effects that are not conventionally corrected for yet. One of the latter are non-tidal loading (NTL) effects: these are non-linear, elastic deformations of the Earth's crust, which are generated by the non-tidal redistribution of masses in the fluid components of the Earth system (e.g., Darwin 1882; van Dam and Wahr 1987; Schuh et al. 2003), i.e., the atmosphere, the oceans, and the continental water storage (hydrology). The corresponding deformations result in instantaneous displacements of the reference points by up to a few cm. This clearly indicates that the accuracy and stability requirements for TRFs—formulated by the Global Geodetic Observing System (GGOS) of the International Association of Geodesy (IAG)—at a level of 1 mm and 0.1 mm/year, respectively, will not be achieved without studying an

improved handling of these non-linear station motions in their realizations.

The correction for NTL effects is hence expected to be beneficial, not least for the determination of the geodetic datum (origin, orientation, scale) of the reference frames. For the JTRF2014, the signals induced by NTL are naturally included in the station position time-series. In the ITRF2014, NTL is not applied directly, but a part of the sum of all non-linear motions is taken into account by estimating and reducing annual and semi-annual signals from the station position time-series (Altamimi et al. 2016). In contrast to that, the DTRF2014 is the first ITRS realization that explicitly uses the displacements generated from geophysical NTL models (for the atmospheric and hydrological components, provided by the chair of the Global Geophysical Fluid Center, GGFC) to correct for the corresponding effects at the normal equation (NEQ) level (Seitz et al. 2021). The phrase "NEQ level" refers to the solution of the normal equation system in the Gauss–Markov model (Koch 1999; Angermann et al. 2004). Accounting for NTL by modifying the NEQs resembles a reduction of the original observations through daily, weekly, or session-wise mean displacements. This procedure offers the possibility to subsequently take into account NTL corrections that were not made at the observation level of the input data (Glomsda et al. 2021).

As shown by Seitz et al. (2021), the application of NTL reduces the root-mean-square (RMS) values of the estimated station positions, and it improves the linear motions for stations with short observation intervals (i.e., less than 2.5 years). Since NTL effects generally have a strong seasonal signal, the correction for the corresponding displacements also reduces the amplitudes of the annual and semi-annual signals in the station positions and consequently in the time-series of the geodetic datum parameters used to realize the ITRF datum, namely the translation and scale time-series.

Therefore, NTL will again be corrected for in the upcoming ITRS realization by DGFI-TUM, the DTRF2020. The amount of available geophysical NTL models has increased in the meantime. Thus, even though there is a data set explicitly designed for the ITRS 2020 realization by the GGFC, we are in principle free to pick the model that copes best with our task, i.e., the correction of input data at NEQ level in a secular reference frame. In this study, we hence compare the GGFC contribution to the ITRS 2020 realization with the NTL data of the Earth System Modelling group at the Deutsches GeoForschungsZentrum (ESMGFZ). We consider the latter, because we already use this data for VLBI analyses (Glomsda et al. 2020), and because it is available on a daily basis, which will enable a timely extrapolation of the DTRF2020. This means an improvement w.r.t. DTRF2014, as the respective site displacements have only been available for epochs up to the year 2015 back then, and extrapolation has to be realized by fitting trigonometric functions to the truncated displacement series. Furthermore, since both data sets include all three NTL components, the DTRF2020 will now contain non-tidal oceanic loading next to the atmospheric and hydrological ones.

In the following, we introduce the two providers and the scope and format of their data. Afterwards, the site displacements induced by the corresponding NTL effects are compared. Since the influence of NTL on geocentre motion is of particular interest for the determination of the TRF origin, the subsequent section is devoted to this topic. Then, we compare the displacement series with the position residuals of GNSS stations. Finally, we assess the properties of the NTL data w.r.t. their applicability in secular reference frames.

Non-tidal loading data

In this section, we describe the origin and format of the NTL data that we considered for application in the DTRF2020.

Global Geophysical Fluid Center

First, there is the GGFC contribution to the ITRS 2020 realization (Boy 2021), which we will abbreviate with GCTI20 in the following. GGFC is a service of the IERS, which collects models describing the effects on Earth's rotation, deformation, and gravity caused by the redistribution of geophysical fluids. These are the fluids of the Earth's interior, as well as air and water on the Earth's surface and in the near-Earth environment. While different (non-tidal) loading data sets are available at GGFC, we only considered GCTI20 (Petrov and Boy 2004; Mémin et al. 2020) for this study. It includes displacements in local directions (North, East, up) of the different components of NTL for all VLBI, SLR, GNSS, and DORIS stations that will be included in the ITRS 2020 realizations. The displacements have a temporal resolution of 1 hour and cover the period from January 1979 or 1980 to June 2021 at the time of writing, but the series is prolongated every few months. Furthermore, they are available for both the centre of mass of the total Earth system (CM) frame and the centre of figure of the solid Earth (CF) frame (for details on these frames, see Blewitt 2003). For each frame, there are five consistently processed displacement file sets:

- ERA5 IB (including or excluding air tides, starting in 1979);

- ERA5 TUGO-m (including or excluding air tides, starting in 1980);
- ERA5 hydro (starting in 1979).

ERA5 is the latest ECMWF (European Center for Medium-range Weather Forecasts; https://www.ecmwf.int/) reanalysis model considering atmospheric pressure, soil-moisture, and snow (Hersbach et al. 2020). The air and water pressure anomalies (i.e., differences from long-term mean pressures) implied by ERA5 are convolved with weighting Green's functions to compute the corresponding elastic displacements at any site of the Earth according to the classic approach described by Farrell (1972) and Petrov and Boy (2004).

ERA5 hydro represents the hydrological component of the NTL, while the other four represent the atmospheric and oceanic components. However, one should only use either ERA5 IB or ERA5 TUGO-m, and each either with or without the air tides. IB is the abbreviation for the Inverted Barometer hypothesis, which assumes that atmospheric pressure changes ΔP_a above the oceans are offset by a change in sea level and hence ocean bottom pressure ΔP_w (van Dam and Wahr 1987; Wunsch and Stammer 1997). The conservation of ocean mass for the IB is achieved by fulfilling Eq. (5) in Petrov and Boy (2004),

$$\Delta P_a + \Delta P_w = \Delta \bar{P}_0, \tag{1}$$

with $\Delta \bar{P}_0$ representing the mean atmospheric pressure over all oceans. With the ERA5 TUGO-m data, on the other hand, the oceans' response to atmospheric pressure is extended by the Toulouse Unstructured Grid Ocean model, which is an update of the model of Carrère and Lyard (2003), according to Boy (2021). The latter is not a static but a hydrodynamic (barotropic) sea level model (Mémin et al. 2020), and mass conservation is achieved with the help of the Boussinesq approximation, i.e., the density of the resting ocean is assumed to be constant in "the appropriate governing equations of motion representing conservation of [oceanic] mass, momentum, and density" (Wunsch and Stammer 1997, p. 84). TUGO-m and IB will provide different results especially at high latitudes and in shallow seas (Carrère and Lyard 2003; Mémin et al. 2020). Finally, there is also an exchange of water between land and the oceans due to evaporation, precipitation, and river flow, for example, and hence ERA5 hydro is enhanced with a mass conservation component as well: uniform ocean layers are added or removed depending on the changes in the land water reservoir (Boy 2021).

Since we are interested in models for the non-tidal effects, we picked the data sets excluding the air tides. A summary of the GCTI20 data is given in Table 1.

Earth System Modelling group in Potsdam

Another provider for NTL data—also listed at GGFC—is ESMGFZ (Deutsches GeoForschungsZentrum 2021). In general, ESMGFZ also generates site displacements following an (optimized) Green's functions approach (Dill and Dobslaw 2013; Dill et al. 2018), but there are several differences w.r.t. GCTI20.

First of all, ESMGFZ applies different underlying numerical (weather) models for non-tidal atmospheric, oceanic, and hydrological loading, respectively:

- ECMWF reanalysis ERA-40 (Kållberg et al. 2004), ERA-Interim (Berrisford et al. 2011), and operational ECMWF data (Hersbach et al. 2018);
- Max-Planck-Institute for Meteorology Ocean Model (MPIOM; Jungclaus et al. 2013);

Table 1 Summary of the non-tidal loading data sets compared in this study

	GCTI20	ESMGFZ
Atmospheric model	ECMWF ERA5	ECMWF ERA-40, ERA-interim, Operational ECMWF
Oceanic model	TUGO-m	MPIOM
Hydrological model	ECMWF ERA5	LSDM
Mass conservation	Included in single components	Separated as sea level loading
Spatial resolution	Selected sites	Global 0.5° × 0.5° grid
Temporal resolution	1 h	3 h (atmosphere, ocean), 24 hours (hydrology, sea level)
Data start epoch	1979/01/01 (ERA5 IB & hydro), 1980/01/01 (ERA5 TUGO-m)	1976/01/01
Update frequency	Every few months	Daily
Frames	CM, CF	CM, CF
Displacements	North, East, up	North, East, up

- Hydrological Land Surface Discharge Model (LSDM; Dill 2008).

The local site displacements (North, East, up) of the three components are stored separately, but not for a predetermined bunch of stations, but on a $0.5° \times 0.5°$ spatial grid, with temporal resolutions of 3 (atmosphere, ocean) or 24 hours (hydrology). However, ESMGFZ also provides a software for interpolating the displacements at any site on the Earth. For the global conservation of mass, ESMGFZ computes a fourth component, the sea level loading. It is generated from solving the sea level equation for the atmospheric mass of the ECMWF models and the terrestrial water storage of the LSDM. Summing up all four components hence leads to a consistent, mass-conserving NTL data set. Like the hydrological component, the sea level loading has a 24 h resolution.

small latency and high spatial resolution, instead of data designed for a particular (and maybe non-permanent) purpose. The big advantage of the ESMGFZ data is the availability of site displacements on a daily basis, which is not given for GCTI20.

Apart from these differences, the site displacements of ESMGFZ are also generated in both the CM- and the CF-frame. Table 1 contains a summary of the data.

Data preparation

CM-frame

We downloaded the time-series of site displacements for GCTI20 (in the CM-frame, excluding air tides) for all VLBI, SLR, GNSS, and DORIS stations relevant for the ITRS 2020 realization. After reducing the resolution from 1 to 3 hours for each time-series, we chose the following categorization according to the common separation of NTL components:

$$\begin{aligned} \text{ERA5 IB} &\rightarrow \text{non-tidal atmospheric loading (NTAL)} \\ \text{(ERA5 TUGO-m) - (ERA5 IB)} &\rightarrow \text{non-tidal oceanic loading (NTOL)} \\ \text{ERA5 hydro} &\rightarrow \text{hydrological loading (HYDL).} \end{aligned}$$

A last important difference to GCTI20 is the fact that the ESMGFZ displacements have not been generated from a single reanalysis set of atmospheric forcing data over their complete history (Dobslaw and Dill 2018). Site displacements are available from January 1, 1976, but the ECMWF reanalysis ERA-Interim data only starts at January 1, 1979. Hence, before that epoch, the reanalysis ERA-40 data were used. ERA-Interim itself is only available until August 31, 2019, so the ECMWF operational data have to be applied after this epoch at the latest. Effectively, ESMGFZ uses the operational data for epochs after 2007.0 already. While the atmospheric surface pressure is adjusted between the distinct products (Dobslaw 2016), other forcing variables like precipitation and evaporation differ significantly between ERA-40, ERA-Interim, and the operational data. The latter itself is subject to model updates, so the operational data contain contingent breaks in these variables as well. As a result, there are transition periods after each change in the ECMWF model, in which the dependent NTL products (all four components, compare Dobslaw and Dill 2018) adapt themselves to the new forcing situation. This is particularly relevant for the hydrological loading (and hence ultimately for the sea level loading), as the LSDM heavily depends on the precipitation in the distinct ECMWF models (Robert Dill and Henryk Dobslaw, personal communication). The reason for not using unique reanalysis data in the first place is a different motivation: ESMGFZ wants to provide operational NTL data with a

As explained above, the IB describes the static effect of atmospheric pressure above the oceans, without taking other oceanic (or wind) dynamics into account. TUGO-m, on the other hand, is a hydrodynamic model and adds sea level variations that are not solely related to atmospheric pressure fluctuations. Hence, it seems reasonable to let the ERA5 IB data represent the non-tidal atmospheric loading, while the non-tidal oceanic loading effect is approximated by the differences between the site displacements for ERA5 TUGO-m and ERA5 IB. Mémin et al. (2020) point out that TUGO-m only represents a part of the NTOL, as it does not consider heat and freshwater fluxes like other, baroclinic, ocean models. However, they show that there is no significant improvement by using the baroclinic models rather than the barotropic TUGO-m for NTOL.

ESMGFZ directly provides the distinct NTL components, so the separation into NTAL, NTOL, HYDL, and sea level loading (SLEL) is trivial. We downloaded the global grids of site displacements in the CM-frame for each component and interpolated the displacements at the same station sites as with GCTI20. Afterwards, the data referring to HYDL and SLEL were interpolated to the same 3 h epoch grid as the NTAL, NTOL, and GCTI20 data.

CF-frame (and geocentre motion)

We did not download and prepare the complete CF-frame data for neither GCTI20 nor ESMGFZ. Instead, we computed the geocentre motion referring to each NTL

component and provider, and used this information to recover the CF-frame displacements from the CM-frame displacements when needed.

Geocentre motion is the time-series of the vector from the centre of figure of the solid Earth, CF, to the centre of mass of the total Earth system including air and water, CM. Put differently, it is the time-series of the position of CM in the CF-frame, where CF = (0, 0, 0). It is generated by the redistribution of mass in the total Earth system, and hence the redistribution of mass in connection with NTL effects contributes to geocentre motion (e.g., Dong et al. 2003). For example, the component $\boldsymbol{g}_{NTAL}(t)$ of geocentre motion referring to non-tidal atmospheric loading at an epoch t is given by the difference between the corresponding site displacements $\boldsymbol{\delta}^{CF}_{NTAL}(t)$ and $\boldsymbol{\delta}^{CM}_{NTAL}(t)$ in the CF- and CM-frames, respectively:

$$\boldsymbol{g}_{NTAL}(t) \quad = \quad \boldsymbol{\delta}^{CF}_{NTAL}(t) \; - \; \boldsymbol{\delta}^{CM}_{NTAL}(t). \qquad (2)$$

In contrast to the original data, these site displacements (and geocentre motion) are now given in the xyz-coordinate system of the ITRS, which means that they must be transferred from the local horizontal frame to the ITRS with rotation matrices $\boldsymbol{R}_s$, which depend on the location of a particular site s.

Any site's displacements can be chosen to compute the geocentre motion contribution, since CM and CF are the same for all sites at the same epoch t. We generated the distinct contributions for both GCTI20 and ESMGFZ by using the CM- and CF-displacements of a subset of 12 globally distributed SLR stations. As expected, the contributions were identical for each of the 12 stations, and the corresponding time-series will be shown in the next but one section. The CF-frame displacements for any site can now be computed from the respective CM-frame displacements with Eq. (2).

Comparison of site displacements

Several studies (e.g., Roggenbuck et al. 2015; Glomsda et al. 2020) have compared NTL data by different providers. In general, the vertical displacements are larger than the horizontal ones for each NTL component by a factor of 2–5 and can reach peak-to-peak variations of 10–30 mm. NTOL usually is the least relevant contributor, except for coastal areas. The models for NTAL mostly agree very well, while those for HYDL tend to show the largest discrepancies. Atmospheric pressure anomalies are rather strong at mid-latitudes and continental sites, while terrestrial water storage (i.e., hydrology) is most relevant near lakes, rivers, and the equator (e.g., Dill and Dobslaw 2013). Thus, there is a latitudinal dependence in particular (compare, e.g., Gobron et al. 2021). All NTL components contain oscillations, and the amplitude is generally largest for the annual signal, especially for HYDL. These general properties pretty much hold for the GCTI20 and ESMGFZ data, too. In the following, we will hence focus on their peculiarities and the difference between CM- and CF-frame.

Atmospheric loading

We defined the ERA5 IB data of GCTI20 to represent NTAL, and hence we compare the corresponding site displacements with those for NTAL by ESMGFZ. In

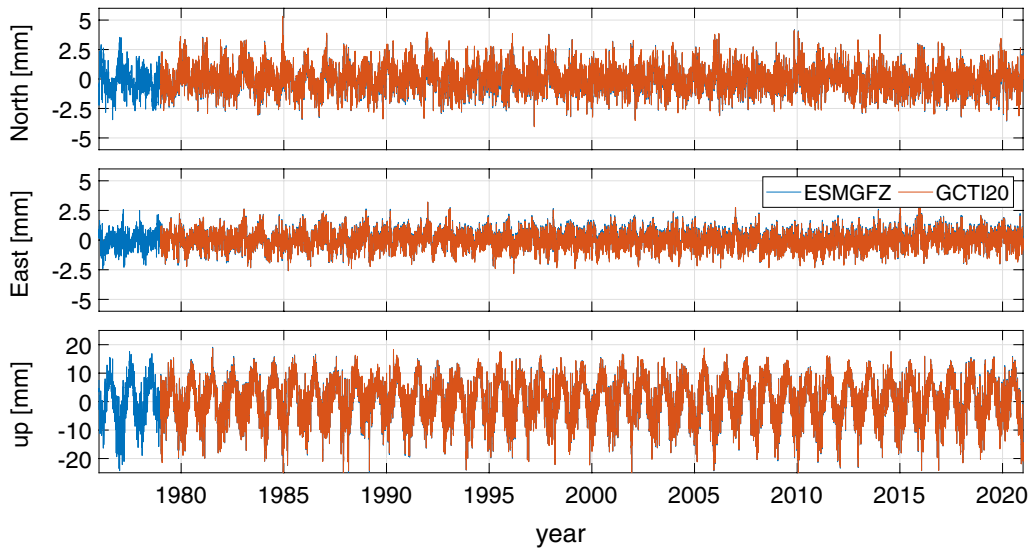

Fig. 1 Site displacements for non-tidal atmospheric loading (NTAL) in the CM-frame at the SLR station 1879 in Altay, Russia. Blue: ESMGFZ, red: GCTI20. Please note the different scale for the up direction

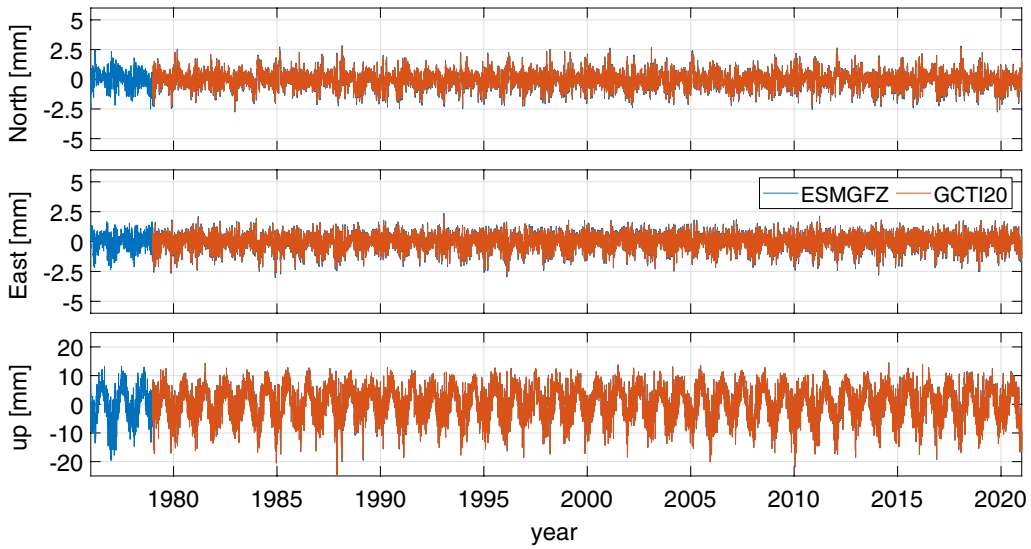

Fig. 2 Same as Fig. 1, but this time the site displacements refer to the CF-frame

Figs. 1 and 2, as for basically all sites, we observe that the respective displacements agree very well between the two providers, for both the CM- and the CF-frame. This is not really surprising, since both GCTI20 and ESMGFZ use ECMWF data, and at least the atmospheric surface pressure in the distinct underlying ECMWF models with ESMGFZ has been adjusted to avoid jumps (compare above). The agreement further confirms that also ESMGFZ makes use of the IB hypothesis for NTAL (Dobslaw and Dill 2018). Displacements in the CF-frame are usually smaller than those in the CM-frame.

Oceanic and hydrological loading

The comparison of the non-tidal oceanic and hydrological components is less straightforward. Previously, we stated that ESMGFZ separates (at least a part of) the mass conservation, i.e., the sea level variation due to atmospheric and hydrological fluctuations, into the SLEL component. GCTI20, on the other hand, considers parts of the mass conservation in both the ERA5 TUGO-m and the ERA5 hydro data. Since we define the NTOL of GCTI20 to be given by the differences in the site displacements for ERA5 TUGO-m and ERA5 IB, and since ERA5 IB is approximately equal to the NTAL of ESMGFZ, we must assume that the oceanic loading of GCTI20 contains a mass conservation part, while that of ESMGFZ does not. Furthermore, Mémin et al. (2020) wrote that TUGO-m only partly includes NTOL. Hence, the NTOL components of the two providers will presumably not match. The same holds for the two HYDL components, as the site displacements for ERA5 hydro in GCTI20 include their mass conservation part, while the conservation part from the hydrological mass loads has been transferred to the SLEL component in case of ESMGFZ.

In Fig. 3, we plotted the RMS values of the differences between the site displacements of GCTI20 and ESMGFZ for the distinct loading components in the CM-frame. Next to the single components NTAL, NTOL, HYDL, and SLEL, we also added the sum of all components per provider. The site displacements refer to the more than 1400 GNSS stations which will be considered in the DTRF2020, and the RMS values are ordered by the latitudinal position of their respective GNSS station. The values are actually smallest for NTAL (compare the previous subsection), with mean values of about 0.1 and 0.2 mm for the horizontal and vertical directions, respectively. As expected, the differences between the ESMGFZ and GCTI20 data increase for NTOL, with RMS values of about 0.7 and 1.1 mm on average. The RMS values for SLEL do not belong to a difference but directly to the time-series of corresponding site displacements by ESMGFZ, since there is no such component provided by GCTI20. Their mean values of about 0.6 and 1.0 mm are similar to those of the differences for NTOL. Finally, the RMS values of differences for a single component are largest for HYDL, a result which was also obtained in previous studies (compare the preliminary remarks of this section): the mean values are 2.3, 1.4, and 4.3 mm for the North, East, and up directions, respectively. The corresponding discrepancy between GCTI20 and ESMGFZ is composed of two parts: (1) the model differences between ERA5 hydro and LSDM, and (2) an ocean mass conservation component which only prevails for GCTI20. Reflecting the proportions between the distinct

components, the RMS values for the combined loading are closest to those for HYDL.

The order by latitude in Fig. 3 reveals some spatial correlation. For the North direction, the overall pattern of the differences between GCTI20 and ESMGFZ resembles a kind of continuous curve, with its maximum values between 30°S and 30°N. While the effect is most pronounced for HYDL, this basically holds for all NTL components. For the East direction, there is hardly any latitude dependence, but for the up direction we can again observe a cluster of large RMS values, this time at about 45°N for HYDL, and about 60°S and 60°N for NTOL. The latter is in line with the study of Gobron et al. (2021), who take other measures but also recognize the strongest impact of non-tidal oceanic (and atmospheric) loading at high latitudes. That is to say, we might expect the differences between GCTI20 and ESMGFZ to be largest in those regions where a particular NTL component is most relevant. For HYDL, these are the low latitudes, which matches the pattern for the North direction at least.

Combined loading

Given the distinct treatment of mass conservation between GCTI20 and ESMGFZ, which is facilitated by the contrast of separated displacements in Fig. 3, it is (apart from NTAL with the IB hypothesis) only consistent to compare the sum of all loading components per provider. Since we are not going to separate the single components in the context of the DTRF2020, this is not a concern at all. In Fig. 4, we plotted the RMS values of the differences in the combined site displacements between GCTI20 (NTAL + NTOL + HYDL) and ESMGFZ (NTAL + NTOL + HYDL + SLEL) for both the CM- and the CF-frame on world maps, which unveil the latitude dependence of Fig. 3 in more detail. We can confirm immediately that the RMS values are generally larger in the CM-frame (left column) and the up direction (bottom row). The largest RMS values for the up direction in both frames are observed in the USA, in Antarctica, and near the equator, especially in South America. This is in line with our statements in the previous subsections, claiming that the largest discrepancies between GCTI20 and ESMGFZ stem from the hydrological models. The rain forest area is particularly sensitive to HYDL, and ERA5 hydro (compare Fig. 3 in Boy 2021) assigns comparatively more hydrological loading to the USA than the LSDM (compare Fig. 2 in Dill and Dobslaw 2013).

In Figs. 5 and 6, we show the time-series of combined site displacements for the GNSS station BRAZ in Brasilia, Brazil. First of all, we observe the usual pattern of the CM-frame displacements (Fig. 5) showing larger peak-to-peak variation than the CF-frame displacements (Fig. 6). The new insight, however, is the presence of distinct drifts and base level offsets for the otherwise seasonal variations. These differ between the providers, between the directions, and between the frames that the displacements have been computed in. Such shifts in trends are critical when NTL is applied in the context of a secular reference frame, as they will be transferred to

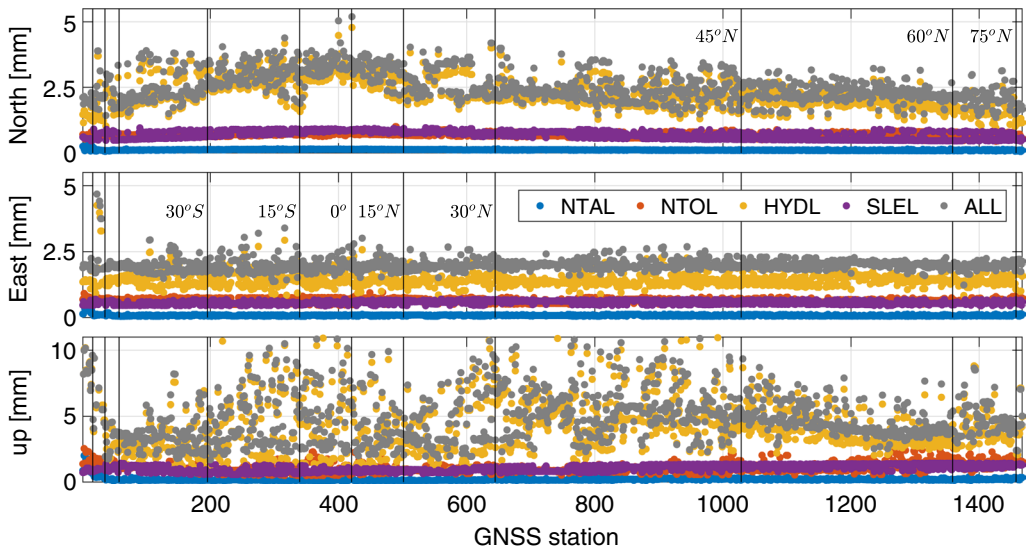

Fig. 3 RMS values of the differences between the site displacements of GCTI20 and ESMGFZ in the CM-frame at GNSS stations, ordered by latitude. Distinct loading components as well as their combination (ALL = NTAL + NTOL + HYDL [+ SLEL]) are considered in the local coordinate system. Please note the different scale for the up direction. The vertical lines indicate the borders between 15° latitude groups

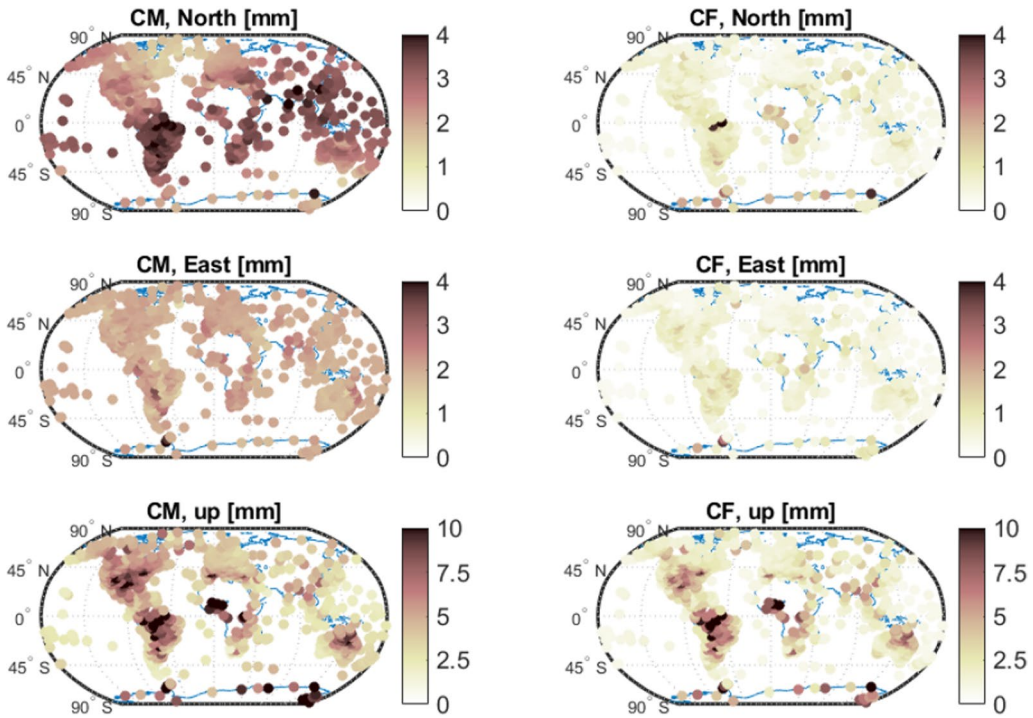

Fig. 4 RMS values of the differences between the site displacements of GCTI20 and ESMGFZ for the combined loading (NTAL + NTOL + HYDL [+ SLEL]) at GNSS stations. Left column: CM-frame, right column: CF-frame. Top: North, middle: East, bottom: up (different scale compared to the horizontal components)

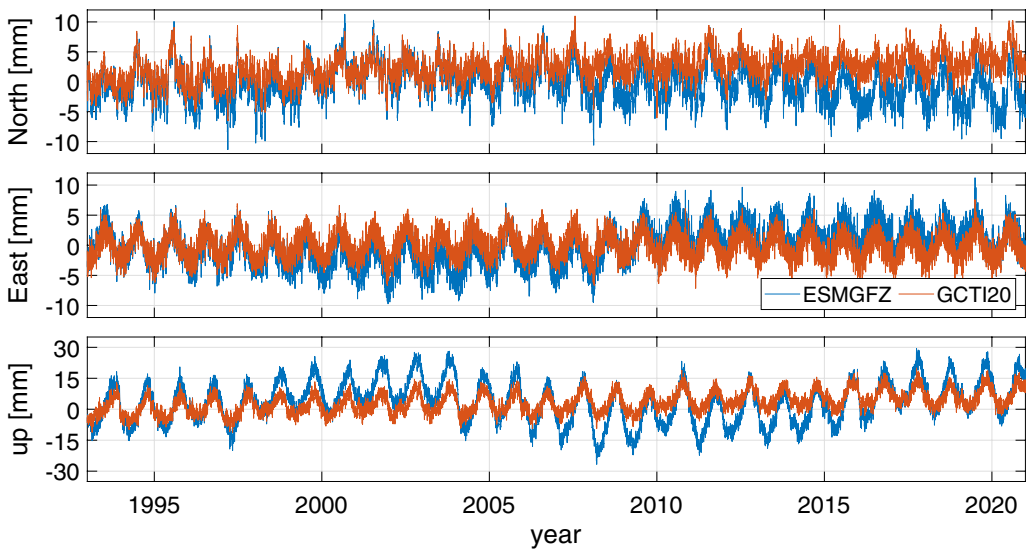

Fig. 5 Site displacements for the combined loading (NTAL + NTOL + HYDL [+ SLEL]) in the CM-frame at the GNSS station BRAZ in Brasilia, Brazil. Blue: ESMGFZ, red: GCTI20. Please note the different scale for the up direction

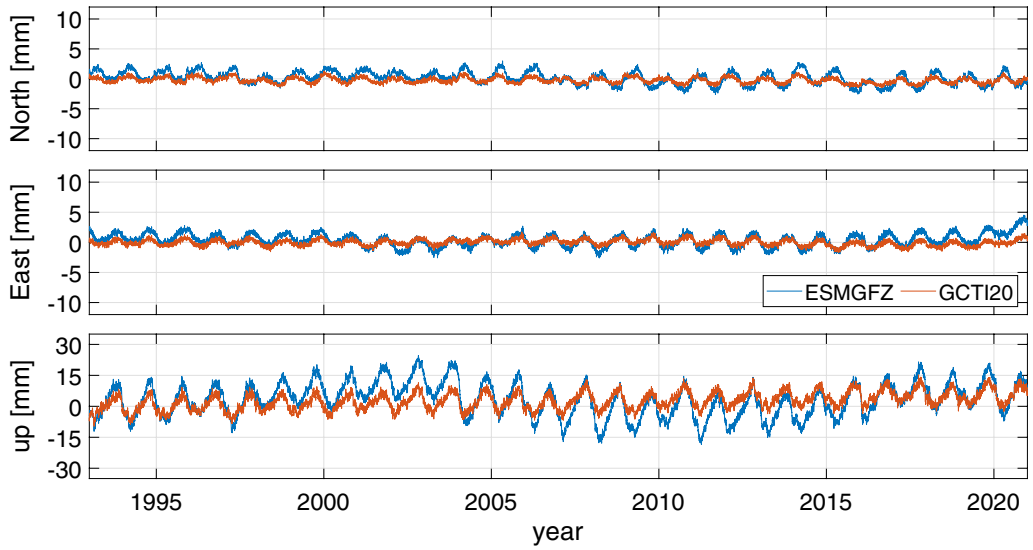

Fig. 6 Same as Fig. 5, but this time the site displacements refer to the CF-frame

the estimated positions and velocities and thus affect the linear motions of the reference points. Hence, we need to investigate the long-term behaviour of the displacement time-series in more detail in the following.

Geocentre motion contribution

Geocentre motion is important for the realization of the origin of the ITRS. The latter is performed with SLR, since CM is the dynamical origin of satellite orbits. When applying NTL in the DTRF2020, the corresponding contribution to geocentre motion hence influences the realized origin. As a consequence, we must analyse the contributions in connection with the site displacements of GCTI20 and ESMGFZ.

Separate loading components

The geocentre motion contributions separated by NTL component are shown in Figs. 7 and 8. For the GCTI20 data (Fig. 7), the motions connected with NTAL and NTOL basically vary around zero without any apparent drift. The seasonal signal is more pronounced for NTAL, especially for the y- and z-coordinates. NTOL, on the other hand, induces a larger contribution than NTAL for the x-coordinate. This might well be related to the diverse land distribution in the x- and y-directions of the TRF. The contribution by HYDL is the smallest for the x- and y-coordinates, and at the same level as NTOL for the z-coordinate. For all coordinates, however, the annual signal of HYDL's contribution is clearly visible, as well as a drift which is quite constant over the whole period from 1980 to 2021. Even though the regional redistribution of land water storage (LWS) is more diverse (e.g., Rodell et al. 2018), these drifts indicate that the global integration of LWS generates a quite stable systematic contribution of HYDL to geocentre motion in the GCTI20 model.

For ESMGFZ (Fig. 8), we observe an analogous behaviour for NTAL and NTOL. The contribution by HYDL, on the other hand, is significantly different. In particular for the x-coordinate, we can identify five major regimes. From 1976 until 1978, the time-series of the respective geocentre motion contribution attains strictly positive values without any significant drift. From 1979 to about 1982, the time-series shows a strong negative drift. From 1983 to about 2009, the negative drift is much smaller, but the time-series values are still mostly positive. Then, at the end of 2009, the values sharply decrease for about one year, before the contribution continues with a small drift and mostly negative values. A similar, but less pronounced pattern is observed for the contribution by SLEL, which is separated for ESMGFZ only. The y- and z-coordinates also reveal changes in offset and drift, but these are less striking than for the x-coordinate. These regimes are most probably related to the transition periods between the distinct underlying ECMWF models, i.e., to the jumps in the corresponding forcing data (mainly precipitation and evaporation), which are driving HYDL and SLEL (compare above).

Combined loading

In Fig. 9, the combined geocentre motion contribution is presented for both GCTI20 and ESMGFZ. It is the sum

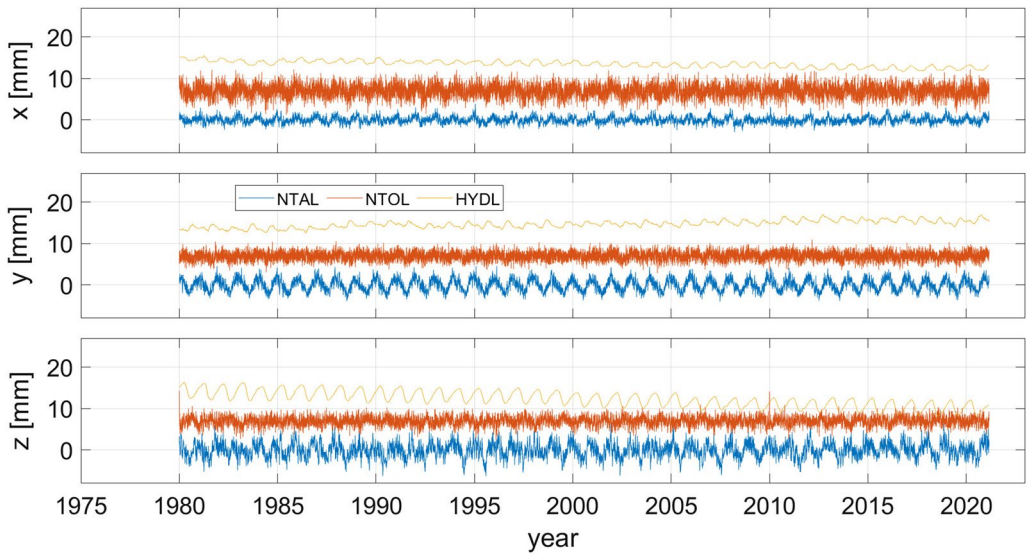

Fig. 7 Geocentre motion connected with the distinct non-tidal loading components of GCTI20. It is computed as the difference between the site displacements in the CF- and the CM-frame according to Eq. (2). The time-series for NTOL and HYDL have been shifted by 7 and 14 mm, respectively

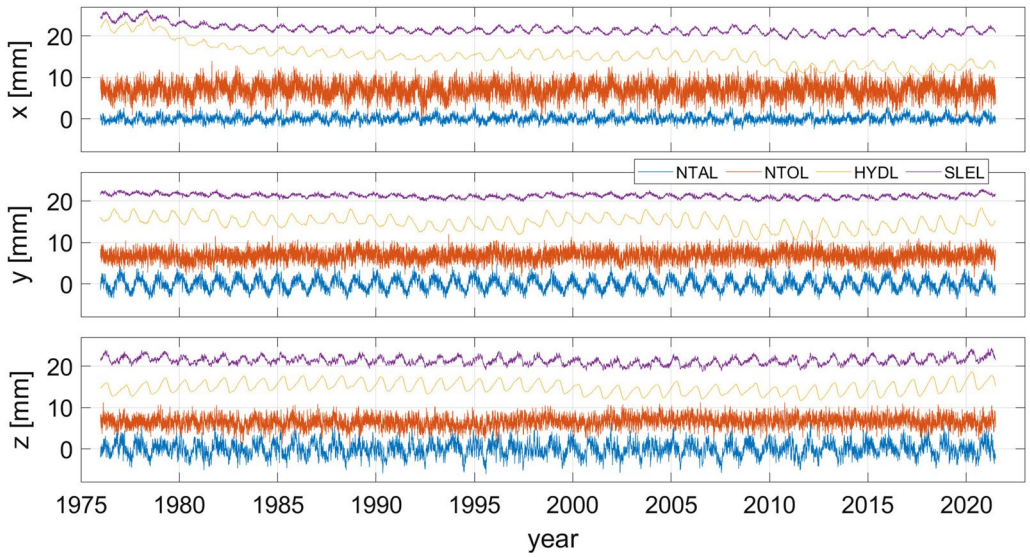

Fig. 8 Same as Fig. 7, but this time the geocentre motion contributions refer to ESMGFZ. Hence, there is an additional component generated by the sea level loading (SLEL), which has been shifted by 21 mm

of the distinct NTL components' contributions, and we can clearly see how the different regimes (trends) for the hydrological and sea level components of ESMGFZ are transferred into the combined contribution. The third geocentre motion contribution in Fig. 9 has been generated from the official SLR solution by the International Laser Ranging Service (ILRS; Pearlman et al. 2019) for the ITRS 2020 realization (Pavlis et al. 2021). It covers the time period between 1983 and 2021 and includes up to four satellites (LAGEOS-1/2, Etalon-1/2), but LAGEOS-1 is the only satellite that was observed before 1993. The contribution is obtained by the network shift approach (e.g., Dong et al. 2003), i.e., by the time-series of translation parameters between the weekly (before 1993: 15-daily) ILRS solutions (CM-frame) and the long-term reference frame that we computed from these solutions (mean CM-frame, i.e., approximately CF-frame). NTL has not been reduced in these solutions, so the resulting

geocentre motion includes NTL effects. However, it also includes other unmodelled geophysical or technique-specific effects, like changes in the SLR observation networks (e.g., Collilieux et al. 2009; Riddell et al. 2017). As a consequence, the ILRS geocentre motion has a less regular pattern and reveals a larger variability, especially for the z-coordinate due to the inhomogeneous station distribution between the northern and southern hemispheres. Before 1993, the variance is even larger for all coordinates, since only one satellite has been observed.

To get some numerical evidence for the long-term behaviour of the distinct geocentre motion contributions, we fitted linear trends to each time-series and listed the corresponding offsets (at 2000.0) and drifts in Table 2. Different start epochs were considered for the fitting intervals:

- 1976.0, the start epoch for the ESMGFZ data;
- 1980.0, the start epoch for the GCTI20 data;

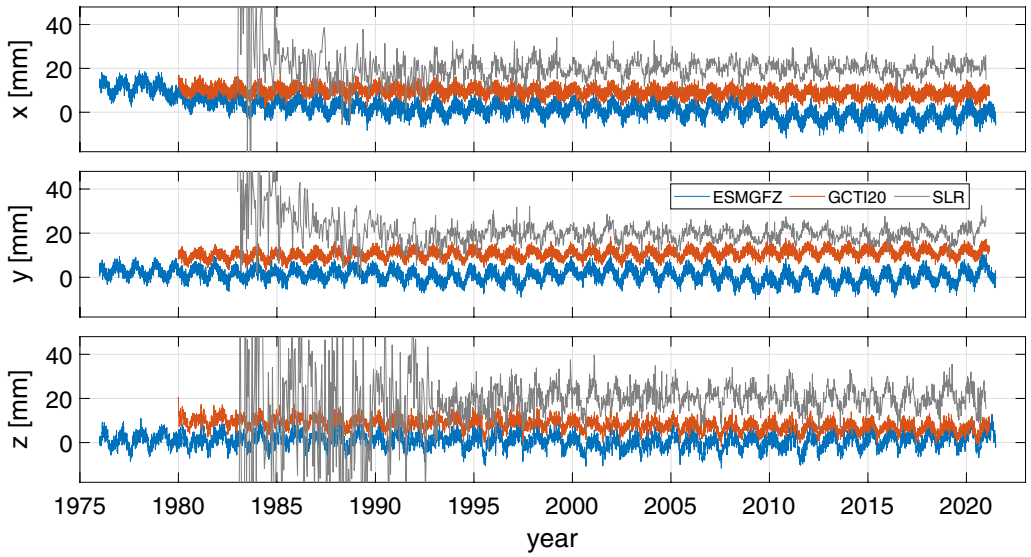

Fig. 9 Geocentre motion contributions as computed for the combined loading of both GCTI20 (NTAL + NTOL + HYDL, red) and ESMGFZ (NTAL + NTOL + HYDL + SLEL, blue). For comparison, also the geocentre motion estimated by SLR is shown (grey). The time-series for GCTI20 and SLR have been shifted by 10 and 20 mm, respectively

Table 2 Fitted trends (offsets at 2000.0 in [mm], and drifts in [mm/year]) for the geocenter motion as computed from ESMGFZ, GCTI20, and ILRS data (see text). In each case, the trends have been fitted from the corresponding time-series period listed in column "period". Formal errors are given in parentheses

Provider	Period	*x*		*y*		*z*	
		Offset	Drift	Offset	Drift	Offset	Drift
ESMGFZ	1976.0–2021.5	1.74 (0.01)	– 0.23 (0.00)	0.83 (0.01)	– 0.06 (0.00)	0.93 (0.01)	– 0.01 (0.00)
	1980.0–2021.5	1.27 (0.01)	– 0.16 (0.00)	0.75 (0.01)	– 0.04 (0.00)	0.91 (0.01)	– 0.01 (0.00)
	1993.0–2021.5	1.48 (0.01)	– 0.17 (0.00)	0.63 (0.01)	– 0.03 (0.00)	0.37 (0.02)	0.04 (0.00)
	2000.0–2021.5	2.07 (0.02)	– 0.22 (0.00)	1.31 (0.03)	– 0.08 (0.00)	– 1.37 (0.03)	0.17 (0.00)
	2010.0–2021.5	– 3.20 (0.07)	0.09 (0.00)	– 4.67 (0.08)	0.28 (0.01)	– 3.94 (0.09)	0.33 (0.01)
GCTI20	1980.0–2021.2	– 0.49 (0.01)	– 0.06 (0.00)	0.69 (0.01)	0.06 (0.00)	– 1.65 (0.01)	– 0.11 (0.00)
	1993.0–2021.2	– 0.48 (0.01)	– 0.06 (0.00)	0.62 (0.01)	0.06 (0.00)	– 1.52 (0.01)	– 0.12 (0.00)
	2000.0–2021.2	– 0.57 (0.02)	– 0.05 (0.00)	0.57 (0.02)	0.07 (0.00)	– 1.97 (0.02)	– 0.09 (0.00)
	2010.0–2021.2	– 0.74 (0.05)	– 0.04 (0.00)	1.70 (0.05)	– 0.00 (0.00)	– 1.88 (0.07)	– 0.09 (0.00)
SLR	1993.0–2021.0	0.21 (0.12)	– 0.00 (0.01)	– 0.58 (0.11)	0.02 (0.01)	– 0.38 (0.18)	0.06 (0.02)
	2000.0–2021.0	0.38 (0.20)	– 0.01 (0.02)	– 0.65 (0.18)	0.02 (0.01)	0.83 (0.30)	– 0.04 (0.02)
	2010.0–2021.0	– 0.12 (0.63)	0.01 (0.04)	– 1.21 (0.63)	0.06 (0.04)	– 0.65 (1.05)	0.05 (0.07)

- 1993.0, the start epoch for the multi-satellite ILRS data;
- 2000.0, an intermediate epoch;
- 2010.0, an apparent discontinuity in the ESMGFZ data.

We observe that the estimated offsets and drifts strongly deviate for ESMGFZ depending on the chosen time period, especially after the years 2000 and 2010. In contrast to that, the trends for the geocentre motion contribution by the GCTI20 data are quite stable, only for the y-coordinate the drift flattens slightly starting in 2010. The geocentre motion estimated from the ILRS solution after 1993 is also rather stable and reveals no significant drifts. Only for the z-coordinate, which is the most variable one as mentioned above, the offsets and drifts show a larger dependence on the time period.

Annual signals

When applying NTL in a secular reference frame, whose origin is realized with SLR, we long for a reduction of the signals in the corresponding geocentre motion. Hence, there shall be a good agreement of the amplitudes and phases of the contributions estimated from the NTL data by GCTI20 and ESMGFZ with those of the ILRS solution. To investigate this, we performed a spectrum analysis of the combined geocentre motion contributions by Fast-Fourier transforms. For consistency, and for leaving out the highly variable period of SLR translations, we only used the time-series starting at 1993.0 for GCTI20, ESMGFZ, and the ILRS solution. However, the spectrum did not change significantly when we considered the full time-series for GCTI20 and ESMGFZ.

The results indicate that the most important signal is the annual one (365.25 days) for all data sets and all directions, and the respective amplitudes and phases are listed in Table 3. For comparison, we also provide the parameters from the study by Wu et al. (2017), who determine geocentre motion by a combination of geodetic and GRACE (Gravity Recovery and Climate Experiment) observations. Looking at the values at large, we observe that neither the GCTI20 nor the ESMGFZ data provide amplitudes and phases that match perfectly with those for the ILRS solution or the solution by Wu et al. (2017). However, considering that the latter two also contain effects other than NTL, the agreement is quite good for individual values (e.g., amplitude and phase of ESMGFZ and ILRS for the x-coordinate, or phase of GCTI20 and ILRS for the z-coordinate). The amplitudes for GCTI20 are always smaller than those for ESMGFZ, but we cannot conclude that one NTL data set will outperform the other w.r.t. this spectrum analysis. Given the dominance of the annual signal for all four geocentre motion contributions, as well as the similarity of the corresponding phases for all three directions, we can nevertheless expect both the GCTI20 and the ESMGFZ data to significantly reduce this signal in geocentre motion.

Comparison with GNSS position residuals

Up to here, we have simply analysed the provided site displacements without any confirmation that they actually agree with the motion of geodetic reference points caused by NTL effects. In this section, we will hence compare the displacements with the (residual) positions of GNSS stations. The impact of NTL on the height of GNSS stations has been studied by various authors, see Tregoning and van Dam (2005) or Williams and Penna (2011), for example. Männel et al. (2019) have even compared these heights with the site displacements of ESMGFZ for the hydrological and a combined (NTAL + NTOL + HYDL) loading.

Time-series statistics

We consider the residuals of a 7 parameter Helmert transformation of daily GNSS station positions (in North, East, and up directions) w.r.t. their linear positions in a combined multi-year GNSS solution. The daily positions have been taken from the 3rd IGS (International GNSS Service; Johnston et al. 2017) reprocessing campaign (repro3; http://acc.igs.org/repro3/repro3.html) and the multi-year solution already incorporates the same

Table 3 Annual amplitudes (in [mm]) and phases (in [d] since January 1st) from a spectrum analysis of the coordinate-wise geocentre motions generated by the combined NTL of ESMGFZ and GCTI20, the ILRS solution, and the unified approach by Wu et al. (2017) (see their Table 1). The corresponding time-series periods are listed in the column "period". Formal errors are given in parentheses

Provider	Period	*x*		*y*		*z*	
		Amplitude	Phase	Amplitude	Phase	Amplitude	Phase
ESMGFZ	1993.0–2021.5	2.70 (0.01)	48.6 (0.01)	3.21 (0.00)	321.1 (0.20)	3.11 (0.02)	44.5 (0.01)
GCTI20	1993.0–2021.2	1.60 (0.01)	23.4 (0.15)	2.12 (0.00)	349.9 (0.20)	2.15 (0.01)	22.1 (0.13)
ILRS	1993.0–2021.0	2.66 (0.15)	46.8 (0.07)	2.53 (0.02)	309.2 (2.73)	3.81 (0.23)	24.8 (1.19)
Wu et al. (2017)	2002.2–2009.0	1.3 (0.1)	46 (4)	3.0 (0.1)	330 (2)	3.3 (0.2)	26 (3)

time-series discontinuities as those that will be applied for the DTRF2020 (we use our own list based on a manual inspection of the time-series). The positions have not been corrected for any NTL, so the corresponding non-linear signals should still be contained in the residual time-series. Furthermore, the residuals refer to the CF-frame, since no information regarding the geocentre motion (by SLR) has been provided to the GNSS solutions yet. Hence, we can only use the site displacements of the CF-frame for comparison.

In Fig. 10, we plotted the position residuals together with the site displacements of GCTI20 and ESMGFZ for the GNSS station SALU in Sao Luis, Brazil. The displacements refer to the sum of all NTL components (NTAL + NTOL + HYDL [+ SLEL]) in the CF-frame. In this example, the match between the residuals and the site displacements is quite good, a fact which cannot be generalized, unfortunately. In particular, the agreement is often rather bad for the horizontal directions. However, the vertical site displacements conform well with the position residuals for many GNSS stations, and the overall impression is that the seasonal amplitudes of the ESMGFZ data match better.

To get the general picture, we computed the correlations between the GNSS position residuals and the site displacements (again for the combined NTL), as well as the RMS values of the differences between them, i.e., of the residuals corrected for the site displacements. For reliability, we only used those DTRF2020 stations whose residual time-series fulfils two conditions: (1) it has a length of at least 2.5 years, and (2) there are at least 250 epochs on average per year. Altogether, 1273 stations pass this filter. Furthermore, we computed the averages of the site displacements within ±0.5 days of the epochs of the residuals (like Mémin et al. 2020), instead of comparing with the snapshot displacement of each epoch only.

In the top row of Fig. 11, we plotted the histograms of the correlations for both providers. For all directions, most of the correlations are positive, indicating a generally common movement of position residuals and site displacements. Negative correlations mainly exist for the horizontal directions (especially for East), and there seems to be a regional cluster in Europe. The correlation values for the horizontal directions are rather small in general, with medians of about 0.24 and 0.26 for ESMGFZ and GCTI20, respectively. For the vertical direction, the correlations are significantly larger, with medians of about 0.46 for ESMGFZ and 0.50 for GCTI20. Hence, the histograms and the median values indicate slightly larger correlations for the GCTI20 data. Männel et al. (2019) have computed similar correlations between their combined ESMGFZ site displacements and the 7 day moving average of their GNSS time-series. While a moving average reduces some noise, we keep the original time-series, as we will apply daily site displacements to daily GNSS normal equations in the DTRF2020. A test calculation showed that the impact on the correlations is not significant, anyway.

In the bottom row of Fig. 11, we show the histograms of the differences

$$\Delta RMS = RMS^{ESMGFZ} - RMS^{GCTI20} \quad (3)$$

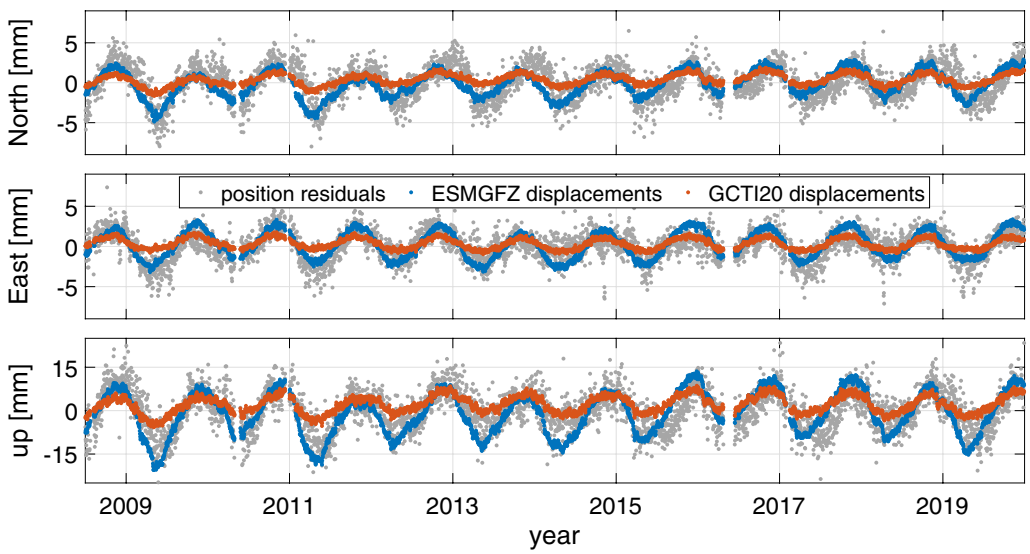

Fig. 10 Position residuals (grey) and combined (NTAL + NTOL + HYDL [+ SLEL]) non-tidal loading site displacements from the CF-frame provided by GCTI20 (red) and ESMGFZ (blue) for the GNSS station SALU in Sao Luis, Brazil. Please note the different scale for the up direction

per GNSS station and local direction, where RMS^p refers to the RMS value of the differences between a station's position residuals and the combined (average) site displacements of provider p. For the horizontal directions, the absolute values of ΔRMS are rather small, and the median is about 0.011 mm. Hence, it does not make a significant difference whether the horizontal position residuals are corrected with the site displacements of GCTI20 or those of ESMGFZ. For the vertical direction, however, the median is about 0.113 mm, indicating a slightly better fit of the GCTI20 data again.

Seasonal signals

The previous subsection left us with the apparent contradiction that the (CF-frame) site displacements of ESMGFZ better match the corresponding GNSS position residuals visually, while the correlations and RMS values suggest a marginally better statistical match for GCTI20. To investigate this in more detail, we fitted the following trigonometric function to the displacement time-series for the combined loading of each GNSS station and provider:

$$\begin{aligned} h(t) \quad = \quad & o \; + \; d \cdot t \; + \; A_1 \cdot \cos\left([t - \phi_1]/T \cdot 2\pi\right) \\ & + \; A_2 \cdot \cos\left([t - \phi_2]/T \cdot 4\pi\right), \end{aligned} \tag{4}$$

with o being an offset, d a drift, A_1 and ϕ_1 the annual amplitude and phase, and A_2 and ϕ_2 the semi-annual amplitude and phase, respectively. t is the epoch in days since 2000.0, and $T = 365.25$ is the number of days per cycle, i.e., in one year.

As can be expected, the estimated offsets and drifts already differ between GCTI20 and ESMGFZ (not shown here). However, the interpretation of these differences is beyond the scope of this paper. At this point, we are more interested in the agreement of the seasonal signals between the displacements and the GNSS position residuals. Hence, we also fitted $h(t)$ to the time-series of these residuals. Although it is widely accepted that GNSS time-series contain temporally variable, i.e., coloured noise (e.g., Zhang et al. 1997; Gobron et al. 2021), we do not apply a sophisticated noise model in the functional fits, amongst others because corresponding information is missing for the displacement time-series, and because it will most likely not change the final results of our comparisons. To obtain the most reliable fits, however, we again restricted ourselves to the 1273 time-series of the previous subsection. In the end, we also dropped those GNSS stations with a formal error greater than 5 days for the estimated annual phase in vertical direction.

In Fig. 12, we plotted the differences between the estimated annual signals for the vertical directions of the remaining 1041 GNSS stations on world maps. In the left column, we compare the annual amplitudes. The mean amplitudes for the vertical displacements of GCTI20 and

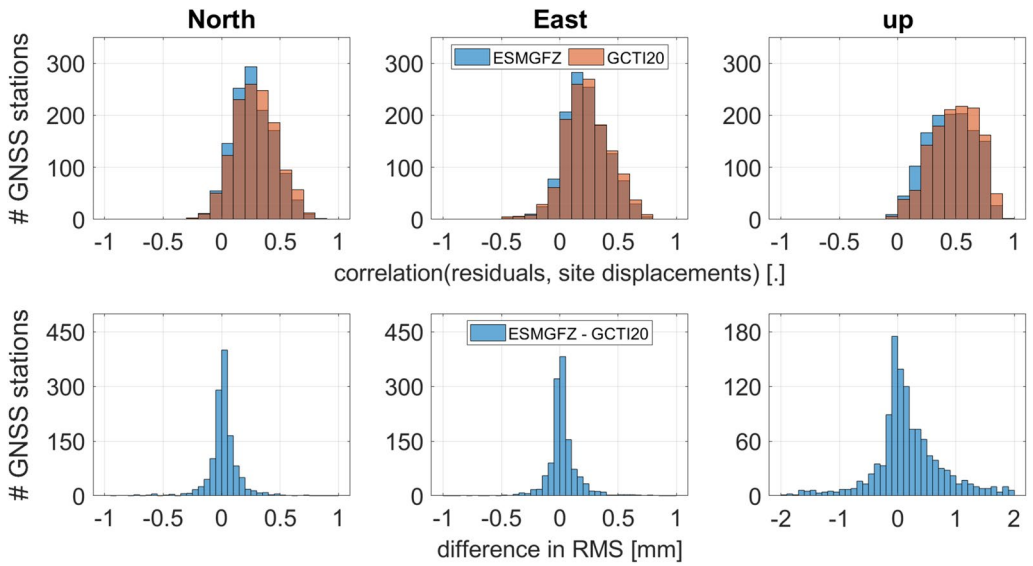

Fig. 11 Top row: histograms of the correlations between GNSS position residuals and the corresponding (24 h average) site displacements for the combined (NTAL + NTOL + HYDL [+ SLEL]) non-tidal loading by either GCTI20 or ESMGFZ. Bottom row: histograms of the differences ΔRMS in Eq. (3). Left column: North, middle column: East, right column: up (different scale for ΔRMS)

ESMGFZ are 2.4 and 3.2 mm for this GNSS station subset, respectively, and most of them differ from the fitted amplitudes for the height residuals (mean value: 3.5 mm) by less than 5 mm. For the largest part of the Earth, in particular Europe, Latin America, East Asia, and Australia, the amplitudes for GCTI20 and ESMGFZ agree very well. The most striking area of disagreement, however, is the Northern part of South America (including the Amazon basin), where HYDL is very strong. Here, the amplitudes partly differ by more than 10 mm, and while the fitted values for ESMGFZ are generally larger than those for the GNSS height residuals, the fitted values for GCTI20 are generally smaller.

In the right column of Fig. 12, the differences between the fitted annual phases are shown. In contrast to the annual amplitudes, they agree particularly well between GCTI20 and ESMGFZ in South America, and differ most in East Asia and at Hawaii. The disagreement with the fitted phases for the GNSS height residuals is largest in Europe and the USA, with a lead of about 50 to 150 days. For about 6% of these stations, the absolute phase lag is actually greater than 100 days. For about 76% of the GNSS stations, the absolute phase lag is smaller than 50 days for both GCTI20 and ESMGFZ, while the fraction of stations with an absolute phase lag of less than 30 days is about 11% larger for the GCTI20 data. Männel et al. (2019) have analysed the connection between GNSS station heights and the ESMGFZ site displacements for HYDL in the Amazon basin, and they also report small phase lags in this region. This might serve as a confirmation, since we can assume that the hydrological loading is the main component of the total one here.

In this context, we observed an interesting pattern when plotting the fitted annual phases for the GCTI20 and ESMGFZ displacements against each other. For each GNSS station, the fitted phase for the ESMGFZ displacements is shown on the x-axes of Fig. 13, while the corresponding fitted phase for the GCTI20 displacements is shown on the y-axes. The majority of the respective plotted dots curls around the line of identity for both frames, CM (blue) and CF (red), confirming the similarity of fitted phases for GCTI20 and ESMGFZ. Beyond that, there is a systematic behaviour, e.g., for the East direction: if the phase of the ESMGFZ displacements for a particular GNSS station is between about 30 and 120 days (or between about 210 and 300 days), then the phase of the corresponding GCTI20 displacements is generally smaller. On the other hand, if this phase is between about 120 and 210 days (or

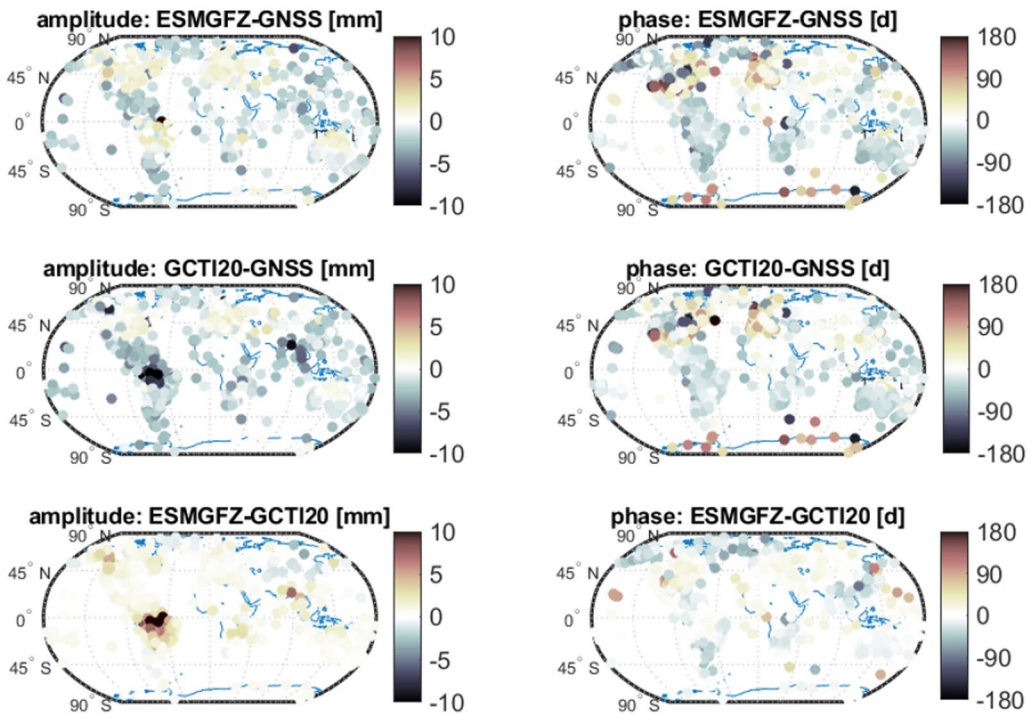

Fig. 12 Differences between the fitted annual amplitudes A_1 (left column) and annual phases ϕ_1 (right column) of Eq. (4) for the vertical displacements of the combined loading (NTAL + NTOL + HYDL [+ SLEL]) of ESMGFZ and GCTI20 in the CF-frame, and for the corresponding GNSS stations' height residuals. Top row: ESMGFZ minus GNSS, middle row: GCTI20 minus GNSS, bottom row: ESMGFZ minus GCTI20

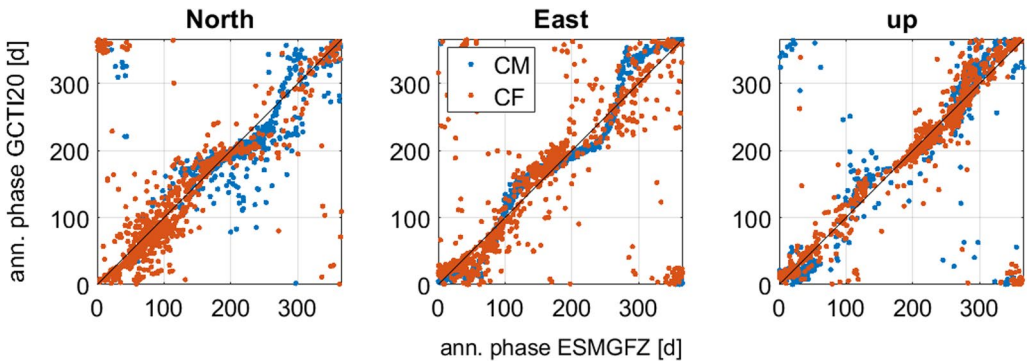

Fig. 13 Fitted annual (ann.) phases in days for the combined (NTAL + NTOL + HYDL + [SLEL]) site displacements of ESMGFZ (x-axes) versus those of GCTI20 (y-axes). Blue dots refer to the CM-frame displacements, and red dots represent the CF-frame displacements

between about 300 and 30 days), then the respective phase for GCTI20 is generally larger. The curve of dots looks sinusoidal, even though the pattern is less pronounced for the North and up directions. The reason for this property probably lies in the peculiarities of the distinct models used by the two providers and is beyond the scope of this paper.

To summarize, discrepancies between the GNSS height residuals and the NTL site displacements arise from both annual phase lags and differences in the annual amplitude. For both GCTI20 and ESMGFZ, one or the other effect is relevant in different regions of the Earth, in particular South America (amplitudes), Europe, and the USA (both: phase lags). In general, the fitted amplitudes for the site displacements of GCTI20 are slightly smaller, so the negative effect—in terms of RMS^{ESMGFZ} and RMS^{GCTI20} from Eq. (3)—of a phase lag w.r.t. the GNSS height residuals is less significant, too. The better statistical match for GCTI20 might be a result of this. However, based on these findings, we cannot conclude that one data set is significantly more accurate for the correction of NTL (in GNSS position time-series).

Assessment w.r.t. the DTRF computation

The main intention of this study is to evaluate the two chosen NTL data sets in terms of their applicability in DGFI-TUM's realization of the ITRS 2020. Besides, it should provide guidance for the decision process of picking any NTL data set for the realization of a secular reference frame. Having described and analysed the data of GCTI20 and ESMGFZ, we will now explain our final choice for the DTRF2020.

Application at the normal equation level

The application of NTAL and HYDL in our previous ITRS realization, DTRF2014, is explained by Seitz et al. (2021). For the DTRF2020, it will basically be the same. The original input data from the International VLBI Service for Geodesy and Astrometry (IVS; Nothnagel et al. 2017), the ILRS, the IGS, and the International DORIS Service (IDS; Willis et al. 2010) for the geodetic space techniques have not been corrected for NTL at the observation level. Hence, we can only correct the input data afterwards at the NEQ level of the weighted least-squares estimation process that we use for the DTRF. (For a detailed description and comparison of the application levels for any site displacements see Glomsda et al. 2021.) This is not an issue, as we are combining the geodetic observations at the NEQ level, anyway. Furthermore, we ensure consistency by applying the same model for all techniques.

To ease the explanation, we provide a few formulas. The DTRF2020 will be a secular reference frame, which means that we are estimating linear motions. For each station (reference point) i, these are represented by an offset vector $\boldsymbol{p}_i$ at some reference epoch t_0 and a constant velocity vector $\boldsymbol{v}_i$, which provide a station position $\boldsymbol{s}_i$ at epoch t by:

$$\boldsymbol{s}_i(t) \quad = \quad \boldsymbol{s}_i(t_0) \, + \, (t - t_0)\, \dot{\boldsymbol{s}}_i \quad =: \quad \boldsymbol{p}_i \, + \, (t - t_0)\, \boldsymbol{v}_i. \tag{5}$$

The correction vectors $\boldsymbol{\Delta p}_i$, $\boldsymbol{\Delta v}_i$ to some a priori vectors $\boldsymbol{p}_i^0$, $\boldsymbol{v}_i^0$ for all stations i are gathered in the vector $\boldsymbol{\Delta x}$ (containing also corrections to other geodetic and auxiliary parameters) and obtained by solving the normal equation system (Koch 1999)

$$(\boldsymbol{N} + \boldsymbol{N}_D)\; \boldsymbol{\Delta x} \quad = \quad \boldsymbol{y} + \boldsymbol{y}_D \quad = \quad \boldsymbol{y}, \tag{6}$$

with normal matrix $\boldsymbol{N}$, normal matrix of datum-conditions $\boldsymbol{N}_D$, and right-hand-side $\boldsymbol{y}$. The right-hand-side of datum-conditions $\boldsymbol{y}_D$ is equal to $\boldsymbol{0}$, since we are using minimum conditions. For the DTRF2020, the final normal matrix (right-hand-side) will contain the sum of many single normal matrices $\boldsymbol{N}_j$ (right-hand-sides $\boldsymbol{y}_j$)

which refer to individual VLBI, SLR, GNSS, and DORIS observation intervals j.

Correcting for NTL at the NEQ level means applying the corresponding (xyz-coordinate) site displacements

$$\boldsymbol{\delta}_j = (\delta_{j1_x}, \delta_{j1_y}, \delta_{j1_z}, \ldots, \delta_{jn_x}, \delta_{jn_y}, \delta_{jn_z}, 0, \ldots, 0) \tag{7}$$

for all stations $i = 1, \ldots, n$ in the following way:

$$\boldsymbol{y}_j^{NTL} = \boldsymbol{y}_j - \boldsymbol{N}_j \boldsymbol{\delta}_j. \tag{8}$$

Hence, the right-hand-side for each observation interval j is reduced by the product of the interval's normal matrix and the vector of site displacements for this interval. $\boldsymbol{\delta}_j$ contains three non-zero values for each station, i.e., one site displacement for each coordinate of their instantaneous positions, which must be a single representative value of the displacements given for the respective observation interval. For VLBI, SLR, GNSS, and DORIS, the relevant observation intervals are (mostly) 24 hours, 1 week or 15 days, 1 day, and 1 week, respectively, and for the DTRF2020 we will apply average values of the corresponding site displacements. The original resolution of the NTL data by GCTI20 is 1 hour, of those by ESMGFZ it is 3 hours (NTAL, NTOL) or 1 day (HYDL, SLEL). As a consequence, both sets can provide at least one value for each technique's observation intervals, and no bridging of gaps is necessary in either case.

Centre of mass vs. centre of figure

The choice of (NTL) site displacements in the CM- or the CF-frame depends on the scope of application. If station positions are given in a CF-frame, and NTL is corrected at the solution level, the site displacements must be taken from the CF-frame as well. If NTL is corrected at the observation level or the NEQ level in VLBI analysis, the frame is irrelevant. This is because the site displacements at the two stations forming a baseline are subtracted from each other, and the geocentre motion is cancelled from the CM-frame displacements, leaving the same difference as for the CF-frame displacements (e.g., Eriksson and MacMillan 2014; Glomsda et al. 2021). Regarding GNSS, Männel et al. (2019) use CF-frame displacements for precise point positioning (PPP) solutions with fixed orbits, and CM-frame displacements for network solutions where the orbits are estimated.

CM is the dynamical origin of satellite orbits, hence the satellite techniques SLR, GNSS, and DORIS are basically able to realize this geocentre. The dedicated SLR satellites are spherical and best suited for determining CM: their cross-section is not attitude dependent, and so they are less affected by non-gravitational forces. The non-spherical GNSS and DORIS satellites, on the other hand, are more sensitive to their actual cross-sections and the non-gravitational forces. Due to aliasing effects, the latter distort the geocentre estimates of GNSS and DORIS solutions (e.g., Bloßfeld et al. 2016). For this reason, Helmert parameters are introduced to restore the degrees of freedom w.r.t. the origin for GNSS and DORIS. When applying NTL in a secular reference frame, the choice of CM- or CF-frame displacements is thus irrelevant for GNSS, DORIS, and VLBI (compare above). For SLR, however, the CM-frame displacements are the only option. Furthermore, CM is the origin of the ITRS, and it is just realized by assuming zero translation w.r.t. the origin of an SLR solution in the ITRS realizations of both IGN (Altamimi et al. 2016) and DGFI-TUM (Angermann et al. 2004; Seitz et al. 2021). As a consequence, and for consistency, we will use CM-frame displacements for all four techniques in the computation of the DTRF2020. Both GCTI20 and ESMGFZ provide these displacements, so either choice of data set is still possible.

Model uncertainties

From the comparison of the NTL data sets, we learned that the agreement of (in particular) the atmospheric and (to a certain extent) the oceanic components is quite good. However, there are significant discrepancies for the hydrological component, and the total NTL displacements do not perfectly match the GNSS position residuals for neither of the two sets. Hence, we must accept for the time being that there is a model uncertainty with respect to the application of NTL effects, especially since there are many other geophysical models and providers of NTL data. A measure of this uncertainty could be the RMS values of the differences between the corresponding site displacements as given in Figs. 3 and 4. Keeping this in mind for the computation of the DTRF2020, we are convinced that the correction for NTL with either of our two data sets will still be beneficial.

Trends in the displacement series

While the NTL data of GCTI20 and ESMGFZ have been deemed to be equivalent for the application in a secular reference frame up to here, we will now explain the reason to favour one over the other.

The modification of the right-hand-sides when applying NTL at the NEQ level, Eq. (8), is derived from the following approximation of the vector $\boldsymbol{f}_j^{NTL}$ of theoretical geodetic observations including the effect of NTL (Glomsda et al. 2021):

$$\boldsymbol{f}_j^{NTL} \approx \boldsymbol{f}_j + \boldsymbol{A}_j\,\boldsymbol{\delta}_j. \tag{9}$$

$\boldsymbol{f}_j$ is the vector of theoretical observations in interval j without considering NTL, and $\boldsymbol{A}_j$ is the matrix of partial derivatives of the functional model f w.r.t. the estimated parameters in $\boldsymbol{\Delta x}$. The site displacements in $\boldsymbol{\delta}_j$ are hence implicitly added to the a priori station positions in interval j, and the corresponding impact of NTL on the theoretical observations in $\boldsymbol{f}_j$ is approximated by the product $\boldsymbol{A}_j\,\boldsymbol{\delta}_j$. In a secular reference frame, the instantaneous station positions from the observation intervals j are turned into long-term linear motions as given in Eq. (5). The application of $\boldsymbol{\delta}_j$ to the a priori values according to Eqs. (8) and (9) changes the instantaneous position estimates. In particular, offsets and drifts in the time-series of site displacements are transferred to the instantaneous positions and will ultimately affect the estimated station offsets $\boldsymbol{p}_i$ and velocities $\boldsymbol{v}_i$.

Trends in the displacement series are either geophysically driven or artefacts which can be attributed to (updates in) the background models. As long as these trends are stable over the entire observation period of each station, both cases can be handled well when computing secular reference frames: the individual offsets and drifts are removed from each displacement time-series, and the correction for NTL is performed with the detrended series. If the trends are real geophysical phenomena confirmed by the geodetic observations, the reduced offsets and drifts will be reflected in the estimated station positions and velocities of the secular frame. Thus, all linear motions are finally contained in the latter and not hidden in the NTL corrections. If the trends are artefacts only, which are not supported by the observations of the geodetic techniques, their reduction from the NTL time-series probably results in unaffected estimated positions and velocities, however.

In contrast, if the trend in a displacement series is not constant over time but changes repeatedly during the observation period of the respective station, the single estimated position and velocity of that station will be significantly distorted. To cope with this situation, there are, in our view, two possibilities. First, one could introduce new station position and velocity parameters whenever the trend in the displacement series changes significantly. This option would contradict the nature of a secular reference frame but facilitates both cases, geophysical and artefact trends, if the corresponding offsets and drifts are again removed from the displacement series between each two discontinuities. The alternative, assuming that trend changes are geophysically caused, is to apply the original displacement series (including all trend changes over the entire observation period of a station) as a correction. However, the estimated station positions and velocities would then only reflect one part of the linear movement, namely the joint long-term one, while all trend variations are included in the NTL corrections. This means that a user would have to re-add the site displacements to the station coordinates to get the actual station motion.

Revisiting the available NTL data in this respect, the current ESMGFZ data are not suitable for the application in DTRF2020. As we have seen in our analyses, their displacement time-series contain various changes in offset and drift over the period from 1976 to 2021 (in particular) in the CM-framework. If these were driven by actual geophysical effects, we would have to decide between introducing station position discontinuities or leaving the trends in the NTL corrections. However, these changes simply are the result of transitions between the various underlying atmospheric forcing models. Hence, applying the original ESMGFZ displacements as a whole is not an option, since this would distort the estimated station positions and velocities. On the other hand, the introduction of additional position and velocity parameters per station for such non-geophysical effects seems to be unjustified and possibly harmful in the context of a secular reference frame.

GCTI20, on the contrary, was processed from consistent underlying models between 1980 and 2021. The corresponding time-series of site displacements do not show any significant intermediate changes in their trends, suggesting that there are not even geophysically induced ones. It follows that single offsets and drifts can be removed from the displacement series which are—after the application of the detrended NTL corrections—properly reflected in the estimated long-term linear motion of each station in the DTRF2020. The purpose of a secular TRF thus has been satisfactorily realized.

Geocentre motion

The behaviour of the geocentre motion contributions shown in Fig. 9 is intrinsically tied to that of the individual displacement time-series. For basically the same reason as given in the previous subsection, the GCTI20 data also has to be preferred over the ESMGFZ data when considering the realization of the DTRF2020 origin with NTL: there are changes in the trend of the geocentre motion contribution for ESMGFZ that are neither geophysically justified nor compatible with the contribution as inferred from the ILRS solution. Instead, they are introduced by the transitions in the underlying atmospheric forcing models and would likely distort the geocentre motion estimated in the DTRF2020. In contrast to that, the trends in geocentre motion as implied by the GCTI20 data are quite stable over the complete time interval (compare Table 2).

Processing of NTL corrections

Following the above assessment, we will apply the CM-frame site displacements of GCTI20 in the DTRF2020. The displacements will be handled in the following way: for each station, the time-series for each NTL component is cut down to the corresponding observation interval. Each such truncated series is detrended, and the respective offsets and drifts are stored for the final DTRF2020 release. The residual time-series are used to compute 15-daily, weekly, or daily averages for each NTL component, which will be part of the release as well. Finally, the sum of all components' averages is computed for each relevant observation interval, and each corresponding input normal equation is corrected for NTL by this sum. As a consequence, the trends in the original displacement series will be reflected by the estimated station positions and velocities of the DTRF2020. After all, this is the ultimate purpose of a secular reference frame: the total linear station motions have to be represented by the (estimated) station velocities.

Since the GCTI20 data will be prolongated every few months, the station positions of DTRF2020 can be extrapolated to future epochs with the aforementioned approach on a regular basis. Together with the separation of trends and the inclusion of NTOL, this is the main difference compared to the preceding DTRF2014 (w.r.t. NTL).

Conclusions

We have compared two non-tidal loading (NTL) data sets: that of the Global Geophysical Fluid Center (GGFC) directly devoted to the ITRS realization 2020 (GCTI20), and the operational one of the Earth System Modelling group of the Deutsches GeoForschungsZentrum (ESMGFZ). With both sets, it is possible to obtain site displacements due to non-tidal atmospheric, oceanic, and hydrological loading for all relevant VLBI, SLR, GNSS, and DORIS stations. Although the data are split into different components, both sets are mass conserving if the sum of all components is considered. The main discrepancy between the data stems from the underlying hydrological models, but it was not our intention to identify the best data in terms of geophysical modelling in this study.

Instead, we analysed which data set is the better choice for usage in DGFI-TUM's upcoming ITRS realization, the DTRF2020. Like the DTRF2014, the new realization will be a secular reference frame, which consists of linear station motions represented by offsets at a specific reference epoch and a constant velocity. Again, we will correct for NTL at the normal equation level (this time including the non-tidal oceanic loading), which is the same level that we use for the combination of the different geodetic space observations.

While we could not distinguish the applicability of the GCTI20 and ESMGFZ data in terms of resolution or the replicability of instantaneous station positions, we finally decided to use the GCTI20 data because of its lack of non-geophysical structure in the corresponding displacement time-series and geocentre motion. For GCTI20, the series generally contain a single trend only, whereas many displacement series and the geocentre motion for ESMGFZ reveal time-dependent offsets and drifts. The latter would distort the estimated station positions and velocities, as well as the realization of the origin of the DTRF2020, as these changes in trends do not reflect real geophysical phenomena, but are induced by updates in the underlying atmospheric forcing models. The resulting time-series of site displacements contain transition periods which cannot be brought into agreement with a secular reference frame. However, this does not impair the appropriateness of the operational ESMGFZ data for other applications.

If, in future ITRS realizations, geophysically caused trend changes are present in the (then) available NTL displacement time-series, the fundamental question of whether discontinuities should be introduced or whether the trend changes should remain in the NTL corrections must be discussed.

Acknowledgements

The authors would like to thank Robert Dill and Henryk Dobslaw at the Deutsches GeoForschungsZentrum for very fruitful discussions on their non-tidal loading data. We also thank Jean-Paul Boy and all other involved colleagues at the Global Geophysical Fluid Center and the Deutsches GeoForschungsZentrum for providing their data and hence enabling this research in the first place. Furthermore, we thank the editor and the two anonymous reviewers for their valuable feedback, which helped to significantly improve our manuscript.

Author contributions

MG, MB, MS, and DA conceptualized the study during the preparation of the DTRF2020. All authors are involved in the corresponding discussions on DTRF procedures and results under the lead of MS. MG prepared the GCTI20 data for analysis, while MB prepared the data by ESMGFZ and the final processing of both data sets for the DTRF2020. MB also computed the geocentre motion contribution of the SLR solution. MS provided the GNSS position residuals. MG performed most of the analyses, with modified scripts originally created by the other authors. FS coordinated the research at DGFI-TUM and provided the basic resources, making the study possible. MG compiled the figures and wrote the manuscript with input by MS, MB, DA, and FS. All authors read and approved the final manuscript.

Funding

Open Access funding enabled and organized by Projekt DEAL.

Availability of data and materials

The GGFC contribution to the ITRS 2020 realization is available at http://loading.u-strasbg.fr/ITRF2020/. The operational non-tidal loading data of ESMGFZ can be obtained from http://esmdata.gfz-potsdam.de:8080/. As soon as the DTRF2020 is generated, the corresponding non-tidal loading data, i.e., offsets, drifts, and residual average site displacements, will be published by DGFI-TUM together with the other components of their ITRS 2020 realization. Any remaining data sets used and/or analysed during the current study are only available from the corresponding author on reasonable request.

Declarations

Competing interests

The authors declare that they have no competing interests.

Received: 21 December 2021 Accepted: 20 April 2022
Published online: 06 June 2022

References

Abbondanza C, Chin TM, Gross RS, Heflin MB, Parker JW, Soja BS, van Dam T, Wu X (2017) JTRF2014, the JPL Kalman filter and smoother realization of the International Terrestrial Reference System. J Geophys Res Solid Earth 122(10):8474–8510. https://doi.org/10.1002/2017JB014360

Altamimi Z, Rebischung P, Metivier L, Collilieux X (2016) ITRF2014: a new release of the International Terrestrial Reference Frame modeling nonlinear station motions. J Geophys Res Solid Earth 121(8):6109–6131. https://doi.org/10.1002/2016JB013098

Angermann D, Drewes H, Krügel M, Meisel B, Gerstl M, Kelm R, Müller H, Seemüller W, Tesmer V (2004) ITRS combination center at DGFI: a Terrestrial Reference Frame Realization 2003, Deutsche Geodätische Kommission, Reihe B, Nr. 313, pp. 1-141. ISBN 3-7696-8593-8

Berrisford P, Dee D, Poli P, Brugge R et al (2011) The ERA-Interim archive Version 2.0. Reading 1:23

Blewitt G (2003) Self-consistency in reference frames, geocenter definition, and surface loading of the solid Earth. J Geophys Res 108(B2):2103. https://doi.org/10.1029/2002JB002082

Bloßfeld M, Seitz M, Angermann D, Moreaux G (2016) Quality assessment of IDS contribution to ITRF2014 performed by DGFI-TUM. Adv Space Res 58(12):2505–2519. https://doi.org/10.1016/j.asr.2015.12.016

Boy J-P (2021) GGFC contribution to the ITRS 2020 realization. http://loading.u-strasbg.fr/ITRF2020/ggfc.pdf. Accessed 16 December 2021.

Carrère L, Lyard F (2003) Modeling the barotropic response of the global ocean to atmospheric wind and pressure forcing - comparisons with observations. Geophys Res Lett 30:1275. https://doi.org/10.1029/2002GL016473

Collilieux X, Altamimi Z, Ray J, van Dam T, Wu X (2009) Effect of the satellite laser ranging network distribution on geocenter motion estimation. J Geophys Res 114:B04402. https://doi.org/10.1029/2008JB005727

Darwin GH (1882) On variations in the vertical due to elasticity of the Earth's surface. Science 14(90):409–427. https://doi.org/10.1080/14786448208628439

Deutsches GeoForschungsZentrum (2021) ESMGFZ Product Repository. http://esmdata.gfz-potsdam.de:8080/. Accessed 16 December 2021.

Dill R (2008) Hydrological model LSDM for operational Earth rotation and gravity field variations, Scientific Technical Report, p. 35, STR08/09, GFZ Potsdam, Germany. https://doi.org/10.2312/GFZ.b103-08095

Dill R, Dobslaw H (2013) Numerical simulations of global-scale high-resolution hydrological crustal deformations. J Geophys Res Solid Earth 118(9):5008–5017. https://doi.org/10.1002/jgrb.50353

Dill R, Klemann V, Dobslaw H (2018) Relocation of river storage from global hydrological models to georeferenced river channels for improved load-induced surface displacements. J Geophys Res 123(8):7151–7164. https://doi.org/10.1029/2018JB016141

Dobslaw H (2016) Homogenizing surface pressure time-series from operational numerical weather prediction models for geodetic applications. J Geod Sci 6:61–68. https://doi.org/10.1515/jogs-2016-0004

Dobslaw H, Dill R (2018) Predicting Earth orientation changes from global forecasts of atmosphere-hydrosphere dynamics. Adv Space Res 61(4):1047–1057. https://doi.org/10.1016/j.asr.2017.11.044

Dong D, Yunck T, Heflin M (2003) Origin of the International Terrestrial Reference Frame. J Geophys Res 108(B4):2200. https://doi.org/10.1029/2002JB002035

Eriksson D, MacMillan DS (2014) Continental hydrology loading observed by VLBI measurements. J Geod 88:675–690. https://doi.org/10.1007/s00190-014-0713-0

Farrell WE (1972) Deformation of the Earth by Surface Loads. Rev Geophys Space Phys 10(3):761–797. https://doi.org/10.1029/RG010i003p00761

Glomsda M, Bloßfeld M, Seitz M, Seitz F (2020) Benefits of non-tidal loading applied at distinct levels in VLBI analysis, J Geod. https://doi.org/10.1007/s00190-020-01418-z

Glomsda M, Bloßfeld M, Seitz M, Seitz F (2021) Correcting for site displacements at different levels of the Gauss-Markov model - a case study for geodetic VLBI. Adv Space Res 68(4):1645–1662. https://doi.org/10.1016/j.asr.2021.04.006

Gobron K, Rebischung P, Van Camp M, Demoulin A, de Viron O (2021) Influence of aperiodic non-tidal atmospheric and oceanic loading deformations on the stochastic properties of global GNSS vertical land motion time series. J Geo Res Solid Earth. https://doi.org/10.1029/2021JB022370

Hersbach H, de Rosnay P, Bell B, et al (2018) Operational global reanalysis: progress, future directions and synergies with NWP. ECMWF. https://doi.org/10.21957/tkic6g3wm

Hersbach H, Bell B et al (2020) The ERA5 global reanalysis. Q J R Meteorol Soc 146:1999–2049. https://doi.org/10.1002/qj.3803

Johnston G, Riddell A, Hausler G (2017) The International GNSS Service, In: Teunissen, Peter J.G. and Montenbruck O. (Eds.), Springer Handbook of Global Navigation Satellite Systems, 1st ed., pp. 967-982. https://doi.org/10.1007/978-3-319-42928-1

Jungclaus J, Fischer N, Haak H et al (2013) Characteristics of the ocean simulations in the Max Planck Institute Ocean Model (MPIOM) the ocean component of the MPI-Earth system model. J Adv Model Earth Syst 5:422–446. https://doi.org/10.1002/jame.20023

Kållberg P, Simmons A, Uppala S, Fuentes M (2004) The ERA-40 archive, Shinfield Park. Reading. https://www.ecmwf.int/node/10595. Accessed Oct 2007.

Koch K-R (1999) Parameter estimation and hypothesis testing in linear models, 2 edn, Springer-Verlag Berlin Heidelberg, original German edition published by Dümmlers, Bonn. ISBN: 978-3-642-08461-4

Männel B, Dobslaw H, Dill R, Glaser S, Balidakis K, Thomas M, Schuh H (2019) Correcting surface loading at the observation level: impact on global GNSS and VLBI station networks. J Geod 93(10):2003–2017. https://doi.org/10.1007/s00190-019-01298-y

Mémin A, Boy J-P, Santamaria-Gómez A (2020) Correcting GPS measurements for non-tidal loading. GPS Solut 24:45. https://doi.org/10.1007/s10291-020-0959-3

Nothnagel A, Artz T, Behrend D, Malkin Z (2017) International VLBI Service for Geodesy and Astrometry - Delivering high-quality products and embarking on observations of the next generation. J Geod 91(7):711–721. https://doi.org/10.1007/s00190-016-0950-5

Nothnagel A, Holst C, Haas R (2019) A VLBI delay model for gravitational deformations of the Onsala 20m radio telescope and the impact on its global coordinates. J Geod 93:2019–2036. https://doi.org/10.1007/s00190-019-01299-x

Pavlis E, Luceri V, Basoni A, Sarrocco D, Kuzmicz-Cieslak M, Evans K, Bianco G (2021) ITRF2020: The International Laser Ranging Service (ILRS) Contribution, presented at AGU Fall Meeting, December 13-17, 2021. https://doi.org/10.1002/essoar.10509208.1

Pearlman MR, Noll CE, Pavlis EC et al (2019) The ILRS: approaching 20 years and planning for the future. J Geod 93(11):2161–2180. https://doi.org/10.1007/s00190-019-01241-1

Petit G, Luzum B (eds.) (2010) IERS Conventions (V.1.3.0), IERS Technical Note 36, Verlag des Bundesamts für Kartographie und Geodäsie, Frankfurt am Main. ISBN 3-89888-989-6

Petrov L, Boy J-P (2004) Study of the atmospheric pressure loading signal in very long baseline interferometry observations. J Geophys Res 109(B3):B03405. https://doi.org/10.1029/2003JB002500

Riddell AR, King MA, Watson CS, Sun Y, Riva REM, Rietbroek R (2017) Uncertainty in geocenter estimates in the context of ITRF2014. J Geophys Res Solid Earth 122:4020–4032. https://doi.org/10.1002/2016JB013698

Rodell M, Famiglietti JS, Wiese DN et al (2018) Emerging trends in global freshwater availability. Nature 557:651–659. https://doi.org/10.1038/s41586-018-0123-1

Roggenbuck O, Thaller D, Engelhardt G, Franke S, Dach R, Steigenberger P (2015) Loading-induced deformation due to atmosphere, ocean and hydrology: model comparisons and the impact on global SLR, VLBI and GNSS Solutions, T. van Dam (eds), REFAG 2014, International Association of Geodesy Symposia, Vol. 146, pp. 71-77, Springer International Publishing Switzerland. ISBN: 978-3-319-45628-7

Schuh H, Estermann G, Crétaux JF, Bergé-Nguyen M, van Dam T (2003) Investigation of hydrological and atmospheric loading by space geodetic techniques. In: Hwang C., Shum C.K., Li J. (eds), Satellite altimetry for geodesy, geophysics and oceanography, International Association of Geodesy Symposia, Vol. 126, pp. 123-132, Berlin: Springer. https://doi.org/10.1007/978-3-642-18861-9_15

Seitz M, Bloßfeld M, Angermann D, Seitz F (2021) DTRF2014: DGFI-TUM's ITRS realization 2014. Adv Space Res. https://doi.org/10.1016/j.asr.2021.12.037

Tregoning P, van Dam T (2005) Atmospheric pressure loading corrections applied to GPS data at the observation level. Geophys Res Lett. https://doi.org/10.1029/2005GL024104

van Dam TM, Wahr J (1987) Displacements of the Earth's surface due to atmospheric loading: effects on gravity and baseline measurements. J Geophys Res 92:1281–1286. https://doi.org/10.1029/JB092iB02p01281

Williams SDP, Penna NT (2011) Non-tidal ocean loading effects on geodetic GPS heights. Geophys Res Lett 38:L09314. https://doi.org/10.1029/2011GL046940

Willis P, Fagard H, Ferrage P, Lemoine FG, Noll CE, Noomen R, Otten M, Ries JC, Rothacher M, Soudarin L, Tavernier G, Valette J-J (2010) The International DORIS Service (IDS): toward maturity. Adv Space Res 45(12):1408–1420. https://doi.org/10.1016/j.asr.2009.11.018

Wu X, Kusche J, Landerer FW (2017) A new unified approach to determine geocentre motion using space geodetic and GRACE gravity data. Geophys J Int 209:1398–1402. https://doi.org/10.1093/gji/ggx086

Wunsch C, Stammer D (1997) Atmospheric loading and the oceanic "inverted barometer" effect. Rev Geophys 35(1):79–107. https://doi.org/10.1029/96RG03037

Zhang J, Bock Y, Johnson H, Fang P, Genrich JF, Williams S, Wdowinski S, Behr J (1997) Southern California permanent GPS geodetic array: error analysis of daily position estimates and site velocities. J Geophys Res 102(B8):18035–18055. https://doi.org/10.1029/97JB01380

Publisher's Note